Development/Plasticity/Repair

# Muscarinic Receptor $M_3R$ Signaling Prevents Efficient Remyelination by Human and Mouse Oligodendrocyte Progenitor Cells

**R. Ross Welliver,[1]* Jessie J. Polanco,[1]* Richard A. Seidman,[1] Anjali K. Sinha,[1] Melanie A. O'Bara,[2] Zainab M. Khaku,[2] Diara A. Santiago González,[2] Akiko Nishiyama,[4] Jurgen Wess,[5] M. Laura Feltri,[1,3] Pablo M. Paez,[1,2] and Fraser J. Sim[1,2]**

[1]Neuroscience Program, [2]Department of Pharmacology and Toxicology, and [3]Department of Biochemistry, Jacobs School of Medicine and Biomedical Sciences, Center for Hearing and Deafness, University at Buffalo, Buffalo, New York 14214, [4]Department of Physiology and Neurobiology, University of Connecticut, Storrs, Connecticut 06269, and [5]Molecular Signaling Section, Laboratory of Bioorganic Chemistry, National Institute of Diabetes and Digestive and Kidney Diseases, National Institutes of Health, Bethesda, Maryland 20892

**Muscarinic receptor antagonists act as potent inducers of oligodendrocyte differentiation and accelerate remyelination. However, the use of muscarinic antagonists in the clinic is limited by poor understanding of the operant receptor subtype, and questions regarding possible species differences between rodents and humans. Based on high selective expression in human oligodendrocyte progenitor cells (OPCs), we hypothesized that $M_3R$ is the functionally relevant receptor. Lentiviral $M_3R$ knockdown in human primary CD140a/PDGF$\alpha$R$^+$ OPCs resulted in enhanced differentiation *in vitro* and substantially reduced the calcium response following muscarinic agonist treatment. Importantly, following transplantation in hypomyelinating *shiverer/rag2* mice, $M_3R$ knockdown improved remyelination by human OPCs. Furthermore, conditional $M_3R$ ablation in adult NG2-expressing OPCs increased oligodendrocyte differentiation and led to improved spontaneous remyelination in mice. Together, we demonstrate that $M_3R$ receptor mediates muscarinic signaling in human OPCs that act to delay differentiation and remyelination, suggesting that $M_3$ receptors are viable targets for human demyelinating disease.**

*Key words:* **CHRM3; demyelination; human; lentivirus; remyelination; transplantation**

**Significance Statement**

**The identification of drug targets aimed at improving remyelination in patients with demyelination disease is a key step in development of effective regenerative therapies to treat diseases, such as multiple sclerosis. Muscarinic receptor antagonists have been identified as effective potentiators of remyelination, but the receptor subtypes that mediate these receptors are unclear. In this study, we show that genetic $M_3R$ ablation in both mouse and human cells results in improved remyelination and is mediated by acceleration of oligodendrocyte commitment from oligodendrocyte progenitor cells. Therefore, $M_3R$ represents an attractive target for induced remyelination in human disease.**

## Introduction

Regenerative therapies that promote remyelination in multiple sclerosis (MS) have the potential to restore lost neurological function and prevent chronic demyelination-associated disease progression. To this end, both enhancing endogenous repair and stem/progenitor cell transplantation have been proposed (Franklin and Goldman, 2015). As quiescent oligodendrocyte progeni-

Received July 3, 2017; revised May 23, 2018; accepted June 17, 2018.

Author contributions: F.J.S. designed research; R.R.W., J.J.P., R.A.S., A.K.S., M.A.O., Z.M.K., D.A.S.G., M.L.F., P.M.P., and F.J.S. performed research; A.N. and J.W. contributed unpublished reagents/analytic tools; R.R.W., J.J.P., R.A.S., A.K.S., M.A.O., and F.J.S. analyzed data; R.R.W., J.J.P., and F.J.S. wrote the paper.

This work was supported by National Institute of Neurological Disorders and Stroke Grant R01NS104021, National Center for Advancing Translational Sciences UL1TR001412, National Multiple Sclerosis Society RG 5505-A-2 and RG 5110A1/1, the Kalec Multiple Sclerosis Foundation, the Change MS Foundation, the Skarlow Memorial Trust, and the Empire State Stem Cell Fund through New York State Department of Health Contract C028108. J.J.P. received additional support from National Institute of General Medical Sciences R25GM09545902 and National Center for Advancing Translational Sciences UL1TR001412-S1. The single-cell RNA-seq was performed by the Genomics Shared Resources at Roswell Park Cancer Institute, which is supported by National Institutes of Health/National Cancer Institute Grants P30 CA016056 (RPCI Cancer Center Support Grant). We thank the Confocal Microscope and Flow Cytometry Facility in the School of Medicine and Biomedical Sciences, University at Buffalo for assistance; and Ted Szczesny and Ed Hurley for assistance with electron microscopy.

The authors declare no competing financial interests.

* R.R.W and J.J.P are co-first authors.

Correspondence should be addressed to Dr. Fraser J. Sim, Department of Pharmacology and Toxicology, School of Medicine and Biomedical Sciences, University at Buffalo, 3435 Main Street, Buffalo, NY 14214. E-mail: fjsim@buffalo.edu.

DOI:10.1523/JNEUROSCI.1862-17.2018

 0270-6474/18/386921-12$15.00/0

tor cells (OPCs) are observed in chronic demyelinated lesions in MS (Wolswijk, 1998; Kuhlmann et al., 2008), induction of differentiation is considered a reasonable pharmacologic approach (Huang et al., 2011a). Similarly, while transplanted human OPCs (hOPCs) have the capacity to myelinate large areas of the hypomyelinated rodent brain, they do so very slowly over several months (Windrem et al., 2008; Wang et al., 2013). Their slow rate of repair likely contributes to the fact that only ~25% of transplant recipients benefit from such treatment. Thus, accelerated differentiation would likely improve the outcome of cell therapy. Indeed, as remyelination acts to protect the demyelinated axons (Irvine and Blakemore, 2008), approaches that accelerate remyelination will yield additional functional benefits by acting to prevent the progressive neurodegeneration that is associated with chronic demyelination (Trapp and Nave, 2008).

Nonselective muscarinic receptor (MR) antagonists have been shown to improve remyelination in rodents (Deshmukh et al., 2013; Mei et al., 2014; Najm et al., 2015). Clemastine, a nonselective MR and $H_1$ histamine receptor antagonist, substantially induced OPC differentiation and remyelination following demyelination in adult spinal cord (Mei et al., 2014). However, clemastine also has potent activity on several other GPCRs, including $\sigma$1/2 (Gregori-Puigjané et al., 2012) and P2X7 (Nörenberg et al., 2011). Likewise, benztropine, a nonselective dopaminergic and MR antagonist, improved remyelination in the cuprizone model of demyelination (Deshmukh et al., 2013). Therefore, for success of future therapy, it is critical to determine which MR subtype or subtypes signal to block oligodendrocyte differentiation and inhibit repair.

Recently, we found that solifenacin, an $M_{1/3}R$ selective antagonist, induced oligodendrocyte differentiation by transplanted hOPCs in a mouse model of hypomyelination (Abiraman et al., 2015). While rat OPCs express all five MRs (Ragheb et al., 2001; De Angelis et al., 2012), in this study, we found that hOPCs only expressed $M_1R$ and $M_3R$. Previous data have demonstrated high $M_3R$ expression in OPCs (Zhang et al., 2014; Abiraman et al., 2015) with little or no expression among other glial cell types (Zhang et al., 2014). Thus, we hypothesized that $M_3R$ signaling in OPCs acts to delay differentiation and, if specifically targeted in OPCs, could induce remyelination. We used genetic approaches in human and mouse OPCs to test this hypothesis. In primary human CD140a/PDGF$\alpha$R$^+$ OPCs, lentiviral (LV) knockdown (KD) of $M_3R$ induced differentiation to postmitotic oligodendrocytes *in vitro* and resulted in precocious myelin formation following transplantation into hypomyelinating *shiverer/rag2* mice. Furthermore, we found that conditional deletion of $M_3R$ in adult NG2-expressing OPCs induced oligodendrocyte differentiation following focal demyelination in mice, likewise leading to improved remyelination.

## Materials and Methods

*Human CD140a/PDGF$\alpha$R cell preparation.* Fetal brain tissue samples, between 17 and 22 weeks of gestational age, were obtained from Advanced Bioscience Resources with consent from patients under protocols approved by the University at Buffalo Research Subjects Institutional Review Board. Forebrain samples were minced and dissociated using papain and DNase as previously described (Conway et al., 2012). Magnetic sorting of CD140a/PDGF$\alpha$R$^+$ cells was performed as described previously (Pol et al., 2013).

*RNA sequencing.* RNA was extracted from $4 \times 10^5$ human CD140a$^+$ OPCs following isolation using EZNA Total RNA Kit I (Omega Bio-Tek) according to the manufacturer's protocols. RNA sequencing was performed at the UB sequencing core on an Illumina HiSeq2500 using 100 cycle paired-end sequencing. Sequences were aligned to the UCSC Hg19 mouse genome using tophat (version 2.1.1), and counts per gene determined using htseq (version 0.6.1). R/Bioconductor was used for subsequent analysis. Following loading of read counts using *DESeq2*, fragments per kilobase per million mapped fragments were calculated. hOPCs isolated from three separate fetal samples between 20 and 21 weeks gestation age were used.

Single-cell RNA-seq was performed on individual CD140a$^+$O4$^+$ OPCs isolated by FACS (Abiraman et al., 2015) using the Fluidigm C1 system per the manufacturer's instructions. To achieve detection of low expressed transcripts, each cell-specific library was sequenced to achieve a depth of $10^6$ transcripts/cell. Single-cell capture was ensured by visual inspection, before lysis and PCR amplification using SMARTER Ultra low RNA kit (Clontech). Quality and quantity of single-cell cDNA were determined by Bioanalyzer HS DNA chip (Agilent Technologies) and PicoGreen assay (Invitrogen). Sequencing libraries were prepared using Nextera XT DNA kit (Illumina), barcoded and sequenced on a HiSeq2500 Sequencer using 100 cycle paired-end sequencing. Bioinformatics was performed as described above.

*shRNAi LV preparation.* TRC shRNAi plasmids targeting CHRM3/$M_3R$ mRNA (TRCN0000011259 and TRCN0000011260) or GFP (TRCN0000072185) were obtained in a pLKO.1 LV vector (Open Biosystems, RHS4533). Lentiviruses were prepared as previously described (Sim et al., 2006). Briefly, following triple transfection of HEK 293T cells with pLKO.1 and packaging plasmids pLP/VSVG (Invitrogen) and psPAX2 (AddGene), viral supernatant was collected at 48 and 72 h, and concentrated by ultracentrifugation. Viral titer was determined by counting colony-forming units following viral infection and selection of HEK 293T cells with 1 $\mu$g/ml puromycin (AMRESCO). KD efficiency was determined in $M_3R$-expressing CHO cells by Western blot, using rabbit IgG anti-$M_3R$ (1:2000, Millipore catalog #AB9018-50UL, RRID: AB_2080197), and in hOPCs by qRT-PCR, as detailed below.

*Infection and puromycin selection.* Following MACS isolation, cells were plated at $5 \times 10^4$ cells/ml in 24-well plates coated with poly-L-ornithine and laminin, in serum-free media (SFM) (Sim et al., 2011) supplemented with 20 ng/ml PDGF-AA (PeproTech) and 5 ng/ml NT-3 (PeproTech). After 24 h, cells were supplemented with 5 ng/ml FGF-2 and infected with $M_3R$ KD or control (TRC GFP shRNAi) lentivirus. The GFP shRNAi was selected as an appropriate control as it represents a validated nontargeting control siRNA that is matched for GC content with $M_3R$ shRNAi (33%–43%). At 24 h after infection, media was replaced with SFM supplemented with 20 ng/ml PDGF-AA and 5 ng/ml NT-3, and cells were allowed to expand for 48 h. Following expansion, cell cultures were additionally supplemented with 400 ng/ml puromycin and allowed to reach ~80% confluence before being passaged for differentiation analysis, calcium imaging, or transplantation into mice.

*Immunocytochemistry.* Puromycin-selected OPCs infected with either $M_3R$ KD or control lentivirus were seeded at $3 \times 10^4$ cells/ml in 24-well plates in SFM supplemented with 20 ng/ml PDGF-AA and 5 ng/ml NT-3. Immunocytochemical analysis was performed as described previously (Conway et al., 2012). Live staining using mouse anti-O4 antibody (1:25) was followed, after fixation, by OLIG2 (1:1000, Millipore catalog #AB9610, RRID:AB_570666). Alexa-488-, Alexa-594-, and Alexa-647-conjugated secondary antibodies (Invitrogen) were used at 1:500 dilutions. Differentiation was assessed as the percentage of O4$^+$OLIG2$^+$ cell of all OLIG2$^+$ cells in culture. Morphological analysis of O4-expressing oligodendrocytes was performed based on criteria described by Huang et al. (2011b). Statistical significance was determined using one-way repeated-measures ANOVA with Tukey's multiple-comparison test (GraphPad Prism 6.0e).

*qRT-PCR analyses.* For qPCR, RNA was obtained following puromycin selection for *in vitro* studies or immediately before transplantation into mice. cDNA was synthesized using SuperScript III reverse transcriptase (Invitrogen). Human-specific primers for SYBR Green-based PCR were described previously (Abiraman et al., 2015). Samples were run in triplicate and gene expression calculated by $\Delta\Delta C_t$ analysis using 18S as a reference. Statistical significance was tested on $\log_2$-transformed data using ANOVA.

*Cloning of LV-EF1a:GCaMP6s.* We PCR/TOPO cloned the coding region of GCaMP6s from pLP-CMV-GCaMP6s-CAAX (AddGene, #52228) (Tsai et al., 2014) into pCR2.1 TOPO4 plasmid (Invitrogen).

The GCaMP6s fragment was then subcloned using unique 5′ SpeI and 3′ PspXI restriction sites into LV pTRIP-EF1a (derived from pTRIP-EF1a; gift of Abdel Benraiss, University of Rochester) (Sevin et al., 2006). Lentiviruses were prepared as described above. Titration of virus was performed on matched mCherry-expressing virus using flow cytometry for mCherry fluorescence and directly compared with GCaMP6s virus using qRT-PCR for WPRE sequence (Geraerts et al., 2006). GCaMP6s expression was confirmed using CHO cells stably expressing the human $M_3R$ (Dörje et al., 1991) by fluorescence imaging following addition of carbachol or $CaCl_2$. For all imaging experiments, hOPCs were infected at one multiplicity of infection for 24 h followed by complete media replacement. One hour before imaging, media was replaced with phenol red-free media.

*Calcium imaging using LV-EF1a:GCaMP6s.* All calcium imaging experiments were performed at 10× using an Olympus IX51 with Prior XYZ stage equipped with a Hamamatsu ORCA-ER camera using a 1× TV lens. All phase images and fluorescent time-lapse acquisitions were performed at room temperature and captured using μManager (Edelstein et al., 2010). Oxotremorine-M (Tocris Bioscience) was thawed immediately before each experiment. Two fields per preparation were imaged for each condition, at 2 s intervals for 10–12 min. Drug addition occurred 1 min after the start of imaging. *Post hoc* immunofluorescence confirmed that 88 ± 1.3% of cells imaged were $Olig2^+O4^-$.

Phase images were used to generate ROIs corresponding to the soma of every cell by thresholding and supervised analysis. Rolling ball subtraction was performed on fluorescence image frames and mean pixel intensity calculated for each cell using ImageJ. Baseline cellular GCaMP6s fluorescence was determined immediately before drug addition on a per-cell basis. Analysis of calcium wave characteristics, such as amplitude, peak number, frequency, and subsequent statistics, was performed in R (complete analysis code is available on request). Briefly, calcium response curves were loess fitted (*zoo*) (Zeileis and Grothendieck, 2005) and the local minima and maxima calculated. Local maxima was considered a peak if its amplitude increased >35% from its local minima. Response duration was measured from the onset of the first peak to the end of the last peak. Area under the curve was calculated for the duration of the response. For each parameter, a linear model was used for two-way ANOVA with Tukey HSD analysis, fitted using virus (control or $M_3R$ KD), oxotremorine dose, and the interaction of these variables as predictors, as well as the source human sample to consider individual tissue sample variability.

*Transplantation into shiverer/rag2 mice.* All animal experiments were performed according to protocols approved by the University at Buffalo Institutional Animal Care and Use Committee. Three fetal brain samples between 17 and 20 weeks gestational age were used for transplantation experiments. Cell preparation and transplantation were performed as described previously (Abiraman et al., 2015). Briefly, hOPCs infected with $M_3R$ KD or control lentivirus were seeded at $\sim 5 \times 10^4$ cells/ml in SFM supplemented with 20 ng/ml PDGF-AA and 5 ng/ml FGF-2, allowed to expand for 48 h, then cultured in SFM supplemented with 20 ng/ml PDGF-AA and 5 ng/ml NT-3 until confluent. Postnatal day 2–3 *shiverer/rag2* mice were anesthetized using hypothermia and $5 \times 10^4$ cells were injected per site, bilaterally at a depth of 1.1 mm into the rostral corpus callosum (~2.5 mm posterior to bregma in day 2–3 pups).

*Analysis of human myelination* in vivo. Animals were killed at 12 weeks after transplant and perfused with 0.9% saline followed by 4% PFA. Cryopreserved coronal sections of mouse forebrain (16 μm) were cut and sampled every 160 μm. Immunohistochemistry was performed, as described previously (Sim et al., 2011). Primary antibodies used were as follows: mouse IgG1 anti-human nuclear antigen (hNA) (1:400, Millipore catalog #MAB1281, RRID:AB_94090), rat IgG2a anti-MBP (1:200, Abcam catalog #ab7349, RRID:AB_305869), mouse IgG2b anti-CC1 (1:50, Millipore catalog #OP80, RRID:AB_2057371), mouse IgG1 anti-human specific GFAP (1:800, Covance Research Products catalog #SMI-21R-500, RRID:AB_509979), and mouse IgG1 anti-neurofilament (1:800, 1:1 mix of Covance Research Products catalog #SMI-311, RRID:AB_2315332 and catalog #SMI-312, RRID:AB_2314902). Goat secondary antibodies were used as described above. Images of entire coronal sections were captured under matching conditions using the 10× objective of an Olympus IX51 with Prior XYZ motorized stage and stitched using Fiji (Schindelin et al., 2012). For each animal, the best cross-sectional region of myelination was determined by blinded assessment of rostral brain coronal sections every 160 μm. Quantification of myelination and differentiation was performed within these areas in each animal. To determine myelination, the portions of $MBP^+$-immunoreactive area ($\mu m^2$) and the number of $hNA^+$ cells were quantified across the corpus callosum. To assess human $CC1^+$ oligodendrocyte differentiation, $CC1^+/hNA^+$ cells were quantified across the corpus callosum. MBP ensheathment of host axons was assessed in the corpus callosum as previously described (Wang et al., 2014). Briefly, a 2 μm stack of 20 optical sections every 0.1 μm was taken, and the proportion of ensheathed axons that crossed 3 perpendicular sampling lines placed randomly over each image was counted (Zeiss LSM 510 Meta confocal).

*$M_3R$ conditional knock-out animals and lysolecithin-induced demyelination.* Young adult (8- to 11-week-old) female Balb/C mice were purchased from Envigo. *NG2creER:Rosa26YFP* animals were a gift from Akiko Nishiyama (University of Connecticut, Storrs, CT) (Zhu et al., 2011). The generation of floxed $M_3R$ mice ($M_3R^{fl/fl}$) has been described previously (Gautam et al., 2006). Animals were bred to generate NG2CreER offspring homozygous for the $M_3R$ floxed allele (*NG2creER:Rosa26YFP:*$M_3R^{fl/fl}$). Conditional gene knock-out by cre-mediated recombination in NG2-positive OPCs was achieved by daily intraperitoneal administration of tamoxifen (200 mg/kg, Sigma-Aldrich) for 5 d, the last of which occurred 7 d before surgery.

Focal demyelination of the young adult (8- to 11-week-old) mouse spinal cord was induced as previously described (Zhao et al., 2006). Briefly, animals were anesthetized under isoflurane (5% for induction, 1.5% for maintenance), and 0.5 μl 1% lysolecithin (Lα-lysophosphatidylcholine, Sigma-Aldrich) was directly injected into the dorsal and ventral funiculi of the spinal cord between two thoracolumbar vertebrae. Preoperative and postoperative analgesia was provided by subcutaneous injection of buprenorphine (0.1 mg/kg).

*Spinal cord processing and analysis by immunohistochemistry and* in situ *hybridization.* Animals were killed at 14 d postlesion (dpl) by transcardial perfusion of saline followed by 4% PFA under deep anesthesia. The spinal column was extracted, postfixed for 30 min in 4% PFA, the spinal cord isolated, cryoprotected in a sucrose gradient (6% sucrose overnight, followed by 15% sucrose overnight), and frozen in OCT medium (Tissue-Tek). Serial 16-μm-thick transverse sections were cut using a Leica cryostat and stored at −80°C.

To identify lesions, one slide from each series was dehydrated in an ethanol gradient, rehydrated, and stained for 15 min in a solution containing 0.2% (w/v) Eriochrome cyanine (Sigma-Aldrich), 5.6% (w/v) $FeCl_3 \cdot 6H_2O$ (Fisher Scientific), and 0.5% (v/v) $H_2SO_4$. Slides were differentiated in 5.6% (w/v) $FeCl_3 \cdot 6H_2O$ until proper depth of color was achieved, dehydrated by sequential ethanol gradient followed by xylene, and mounted in OpticMount I (Mercedes Medical). Slides immediately adjacent to the lesion centers were used for all immunohistochemical and *in situ* hybridization procedures. Additional primary antibodies were as follows: mouse anti-Gfap (1:300, Millipore catalog #MAB360, RRID:AB_11212597), rabbit anti-Iba1 (1:300, Wako catalog #019-19741, RRID:AB_839504), and rabbit anti-Ng2 (1:200, Millipore catalog #AB5320, RRID:AB_91789). *In situ* hybridization, using digoxigenin-labeled *Plp1* antisense RNA probe (Fancy et al., 2004), was performed as described by Sim et al. (2002). The density of positive labeled cells was calculated at 20× magnification following imaging and montaging of entire spinal cord sections. White matter lesions with cross-sectional area <10,000 $\mu m^2$ were excluded from the analysis, as were lesions that extended into the gray matter. Analysis was performed by an investigator blinded to the identity of the sections.

*Electron microscopy.* Mice were perfused with 4% glutaraldehyde and spinal cords removed ($n = 5$ per group); 1-mm-thick blocks surrounding the spinal cord lesion were processed through osmium tetroxide, dehydrated through ascending ethanol washes, and embedded in TAAB resin (TAAB Laboratories). The 1 μm sections were cut, stained with 1% toluidine blue (Sigma-Aldrich), and examined by light microscopy. Selected blocks were trimmed, ultrathin sections cut, and examined by electron microscopy (Hitachi, H600). Images were acquired at 2900× magnification. Analyses of remyelinated axons and *g*-ratios were performed blinded. For remyelination counts, a minimum of 300 axons

were counted for each animal from at least six different fields, with 3 or 4 animals per treatment group. Analysis of *g*-ratios represents 200 axons from each animal.

*Experimental design and statistical analysis.* The following experimental design was followed for *in vitro* experiments assessing the effect of M3R KD on hOPC differentiation. Three experimental groups were tested (control, M3R A, and M3R B) at a single time point with immunocytochemical and RNA-based endpoints. As cultures were tested from matched individual human tissue samples, comparison between individual groups was performed by repeated measures one-way ANOVA followed by Dunnett's *post hoc* tests. Calcium imaging experiments consisted of two independent experimental variables: oxotremorine dose and virus ($M_3R$ KD vs control virus). As such, two-way ANOVA was used with Tukey HSD post tests. In animal experiments, two experimental groups were tested (control or M3R deletion, either shRNAi or conditional knock-out). Student's *t* tests were performed to compare distinct experimental endpoints. Group sizes can be found in the experimental corresponding Results section. Statistical analyses were performed in GraphPad Prism (version 6.0e), or for calcium imaging experiments using R (3.4.3).

## Results

### $M_3R$ expression in hOPCs delays onset of oligodendrocyte differentiation *in vitro*

We recently found that the $M_3R$ was the most differentially expressed G-protein coupled receptor in human CD140a$^+$O4$^+$ OPCs (Abiraman et al., 2015). To better determine the expression of MR subtypes, we performed RNA-seq analysis of CD140a$^+$-sorted OPCs. Among the five MR subtypes, only $M_1R$ and $M_3R$ were expressed at detectable levels by human CD140a$^+$ OPCs (3.1 ± 0.5 and 3.0 ± 0.4; mean ± SEM; fragments per kilobase per million mapped fragments, respectively, RNA-seq, $n = 3$ individual patient samples). To define whether $M_3R$ was expressed by all OPCs or in a heterogeneous pattern, we performed single-cell RNA-seq (Fluidigm C1). Intriguingly, among single CD140a$^+$O4$^+$ FACS-sorted OPCs, we detected $M_3R$ in 13 of 48 cells but could not detect $M_1R$ with this method. Based on these expression data, we focused on $M_3R$ function and hypothesized that $M_3R$ signaling acts to delay differentiation of human primary OPCs.

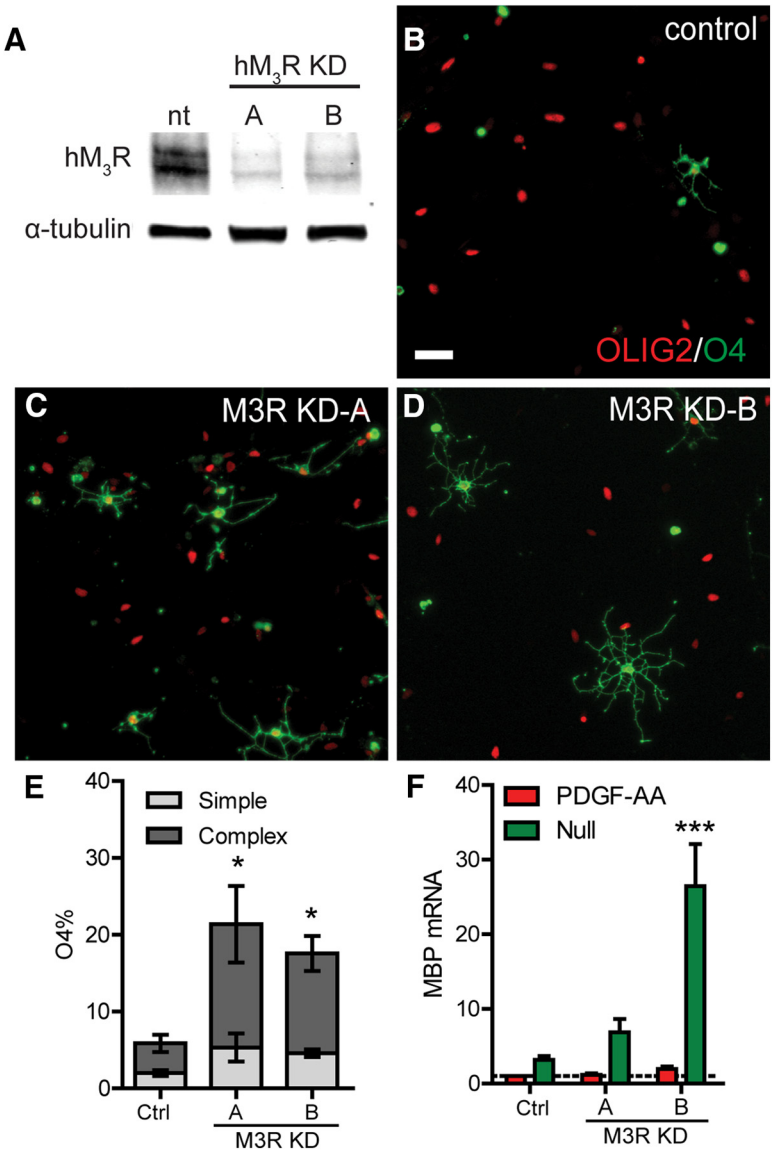


**Figure 1.** $M_3R$ KD induces human CD140a/PDGF$\alpha$R$^+$ OPC differentiation *in vitro*. ***A***, Western blot confirmation of $M_3R$ KD by LV shRNAi in CHO-$M_3R$ cells. ***B–D***, Fetal PDGF$\alpha$R/CD140a$^+$ hOPCs were infected with $M_3R$ (***A***, ***B***) or control shRNAi LV, selected with puromycin and switched to mitogen-free media to encourage oligodendrocyte differentiation. Oligodendrocyte differentiation, determined by the proportion and morphological complexity of O4$^+$ oligodendrocytes (green) and OLIG2$^+$ cells (red), was increased in $M_3R$ KD hOPCs (***B–D***, quantified in ***E***, mean ± SEM). MBP qRT-PCR, normalized to control OPCs in PDGF-AA, showed increase myelin protein gene expression following $M_3R$ KD (***F***, mean ± SEM). *$p < 0.05$ versus Ctrl (two-way ANOVA followed by Bonferroni *post hoc* test). ***$p < 0.001$ versus Ctrl (two-way ANOVA followed by Bonferroni *post hoc* test). There were 3 fetal samples (18- to 20-week gestational age). Scale bar, 20 $\mu$m.

We used LV-mediated shRNAi KD to genetically ablate $M_3R$ expression and signaling in hOPCs. Following a screen of several shRNAi vectors in $M_3R$-expressing CHO cells, we found that two distinct $M_3R$ shRNAi vectors, labeled A and B, significantly reduced $M_3R$ mRNA (CHRM3 qPCR, *post hoc* $p = 0.002$ and $p = 0.01$, respectively, $n = 3$) and protein (Fig. 1). Similarly, these two shRNAi vectors induced a significant KD of $M_3R$ in CD140a/PDGF$\alpha$R$^+$ hOPCs (36.0 ± 12.2% and 56.3 ± 8.9% KD for A and B, respectively, $n = 4–6$) relative to nontargeted control siRNA. Importantly, $M_1R$ expression was not affected following $M_3R$ KD ($M_1R$ expression ratio vs control infected cells was 0.83 ± 0.69 and 1.07 ± 0.19 following infection with shRNAi A and B, respectively; $n = 3$, $p > 0.7$, Dunnett's *post hoc*).

Next, to determine whether $M_3R$ KD would influence hOPC differentiation *in vitro*, we infected freshly isolated CD140a$^+$ fetal hOPCs with $M_3R$ KD or control virus, performed puromycin selection, and switched the resulting cultures to mitogen-free media to promote oligodendrocyte differentiation. After 4 d, the proportion of O4$^+$ oligodendrocytes differentiating from $M_3R$ KD-infected hOPCs (33.9 ± 8.0% and 30.9 ± 10.9% for A and B, respectively) was significantly increased compared with nontargeted control cells (10.9 ± 5.0%, Tukey's *post hoc* adjusted $p = 0.01$ and 0.03, $n = 5$; Fig. 1*B–E*). In addition, we observed substantially more O4$^+$ cells with a complex branched morphology

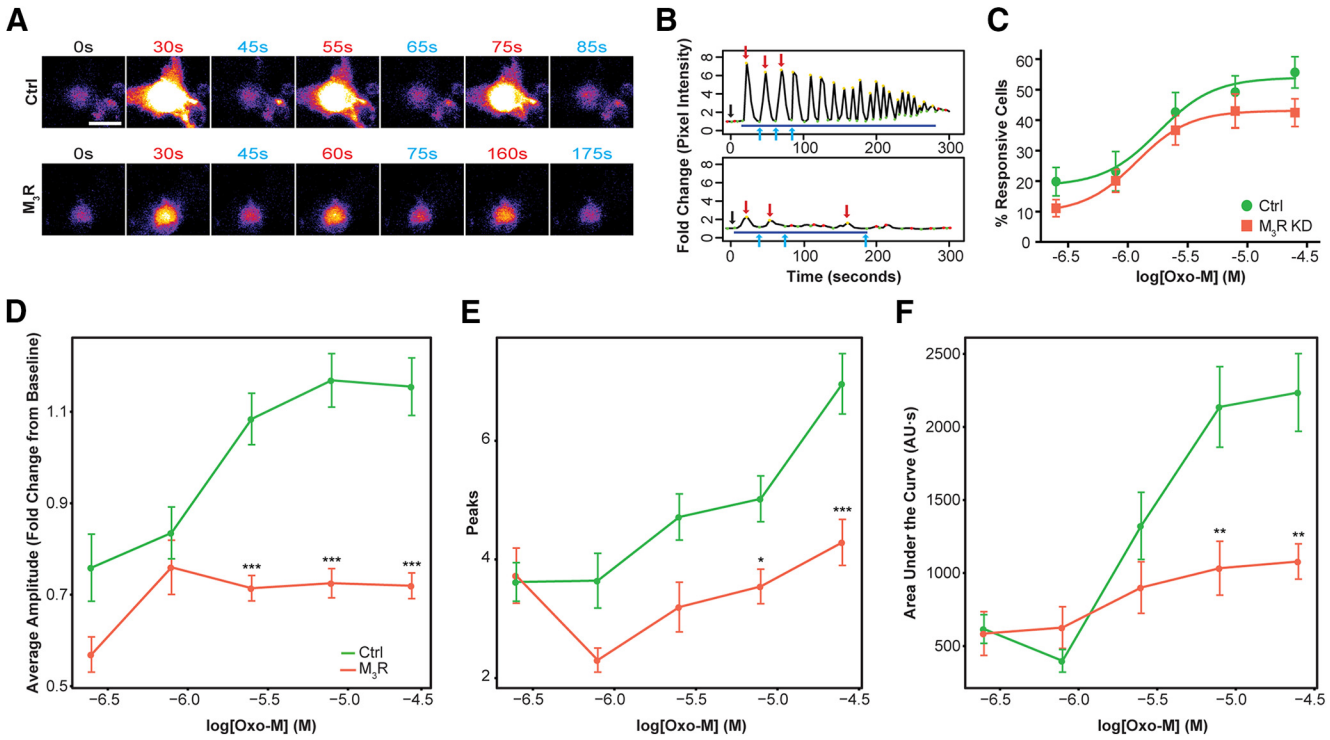


**Figure 2.** $M_3R$ modulates muscarinic-evoked $Ca^{2+}$ response in hOPCs. Fetal CD140a$^+$ hOPCs were cultured and infected with intracellular $Ca^{2+}$ reporter GCaMP6s and $M_3R$ or control shRNAi LV. Time-lapse microscopy of $Ca^{2+}$ response following Oxo-M treatment was recorded and analyzed. ***A***, Pseudo-color representation of $Ca^{2+}$ response from control (top) and $M_3R$ KD (bottom) hOPCs. ***B***, Normalized intensity plots for control (top) and $M_3R$ (bottom) KD hOPCs. ***C***, Dose–response curves of percentage $[Ca^{2+}]_i$ responding cells following Oxo-M addition. Per-cell quantification of average $Ca^{2+}$ peak amplitude (***D***), total number of $Ca^{2+}$ spikes (***E***), and area under the curve (***F***) in $Ca^{2+}$-responsive hOPCs. $M_3R$ KD (red) resulted in a highly significant decrease in $Ca^{2+}$ response at higher Oxo-M doses. *$p < 0.05$ (two-way ANOVA with Tukey's HSD post test). **$p < 0.01$ (two-way ANOVA with Tukey's HSD post test). ***$p < 0.001$ (two-way ANOVA with Tukey's HSD post test). There were two fetal preparations ($n > 30$ cells per condition/dose, mean ± SEM). Scale bar, 25 $\mu$m.

(Fig. 1*E*), consistent with more advanced differentiation in $M_3R$ KD-transduced cells. In hOPCs cultured in the presence of PDGF-AA, $M_3R$ KD was not sufficient to induce oligodendrocyte differentiation. MBP mRNA was not significantly upregulated in either control or $M_3R$ KD groups unless cultured in differentiating conditions (Fig. 1*F*). However, whereas control cells exhibited a threefold increase in MBP in the absence of PDGF-AA, $M_3R$ KD cells upregulated MBP by >25-fold, indicating that $M_3R$ signaling acts to slow synthesis of myelin gene protein mRNA as well as morphological maturation.

### $M_3R$ regulates the calcium response following muscarinic agonist treatment in hOPCs

We next sought to determine the contribution of $M_3R$ on downstream signaling in OPCs following MR activation. Muscarinic agonist treatment of hOPCs results in robust intracellular calcium release (Cohen and Almazan, 1994; Haak et al., 2001). To determine the contribution of $M_3R$ signaling in muscarinic-evoked $Ca^{2+}$ responses, we tested whether $M_3R$ KD in hOPCs altered intracellular $Ca^{2+}$ release using LV GCaMP6s (Chen et al., 2013). Upon muscarinic agonist treatment (oxotremorine-M; Oxo-M), GCaMP6s fluorescence rapidly increased in hOPCs (Fig. 2), indicative of an increase in intracellular $Ca^{2+}$ concentration $[Ca^{2+}]_i$. The vast majority of responding cells (>85%) exhibited a distinctly oscillatory pattern of $[Ca^{2+}]_i$ response lasting up to 5 min in duration (Fig. 2*A*,*B*). The proportion of responding hOPCs increased in a dose-dependent manner in both control and $M_3R$ KD cells (Fig. 2*C*). While we noted a downward shift in the dose–response curve for $M_3R$ KD cells, $M_3R$ KD did not affect the $EC_{50}$ of Oxo-M ($\log(EC_{50}) = -5.74 \pm 0.20$ vs $-5.93 \pm 0.18$ for control and $M_3R$ KD, respectively; two fetal preparations, $n > 30$ cells per condition/dose). This is consistent with shRNAi-mediated reduction in $M_3R$ receptor expression leading to a reduction in signaling efficacy while not altering the ligand/receptor affinity.

Interestingly, among activated oscillating hOPCs, $M_3R$ KD led to a striking attenuation of $Ca^{2+}$ spike amplitude following muscarinic stimulation (Fig. 2*D*). This resulted in a complete loss of dose dependency for average peak amplitude and highly significant reduction on spike amplitude in $M_3R$ KD hOPCs (Tukey's HSD; 2.5 $\mu$M, $p = 0.00013$, 7.9 $\mu$M, $p = 1.5 \times 10^{-11}$, 25 $\mu$M, $p = 3.1 \times 10^{-9}$). The minimal response observed in $M_3R$ KD cells could correspond to activity of residual $M_3R$ expression or to activity of other receptors, such as $M_1R$. While response duration and frequency were only mildly reduced, $M_3R$ KD induced a highly significant decrease in the total number of $Ca^{2+}$ spikes elicited by Oxo-M at higher doses (Fig. 2*E*). The combination of these alterations in $[Ca^{2+}]_i$ response profile translated into a significant difference in the total cellular calcium response, as assessed by the area under the curve (Fig. 2*F*). Together, these data indicate that $M_3R$ is critical in mediating the muscarinic agonist-induced $Ca^{2+}$ response in hOPCs.

### $M_3R$ KD promotes oligodendrocyte differentiation following transplantation into hypomyelinating *shiverer* mice

Next, we investigated whether $M_3R$ signaling is active in hOPCs *in vivo* and acts to impair remyelination by transplanted human cells. hOPCs infected with control or $M_3R$ KD LV were transplanted into neonatal hypomyelinated *shiverer/rag2* mice ($10^5$ cells per animal) as described previously (Abiraman et al., 2015).

Twelve weeks after implantation, transplanted human engrafted hOPCs were widely distributed within the recipient corpus callosum and had begun to differentiate into MBP-expressing oligodendrocytes (Fig. 3). Similar to observations with pharmacological MR antagonists (Abiraman et al., 2015), $M_3R$ KD did not significantly influence the density of human $hNA^+$ cells (958 ± 121 vs 764 ± 66 $hNA^+$ cells/$mm^2$ for $M_3R$ KD and control, respectively, $n = 3$).

Importantly, $M_3R$ KD significantly increased the production of human oligodendrocytes ($hNA^+CC1^+$: 309 ± 71 vs 133 ± 33 $CC1^+hNA^+$ cells/$mm^2$ for $M_3R$ KD and control, respectively, $p = 0.034$, $n = 3$; Fig. 3*B*,*C*). The extent of human oligodendrocyte maturation and myelination was measured by MBP immunostaining, which is completely absent in *shiverer* mice. The increased density of human oligodendrocytes resulted in substantially more MBP-positive fibers in animals receiving $M_3R$ KD-infected cells (Fig. 3*A*,*D*,*E*). Within the corpus callosum, the area of $MBP^+$ immunostaining per human cell was increased by >5-fold in $M_3R$ KD recipients ($p = 0.033$, $n = 3$; Fig. 3*E*). Moreover, when quantified by confocal microscopy, $M_3R$ KD in transplanted hOPCs resulted in a 30% increase in the fraction of ensheathed axons within engrafted regions of the corpus callosum (54.2 ± 3.8% vs 41.7 ± 1.2% for $M_3R$ KD and control, respectively, *t* test, $p = 0.034$, $n = 3$; Fig. 3*F*,*G*). Together, these data demonstrate that $M_3R$ signaling delays hOPC differentiation and myelination *in vivo*.

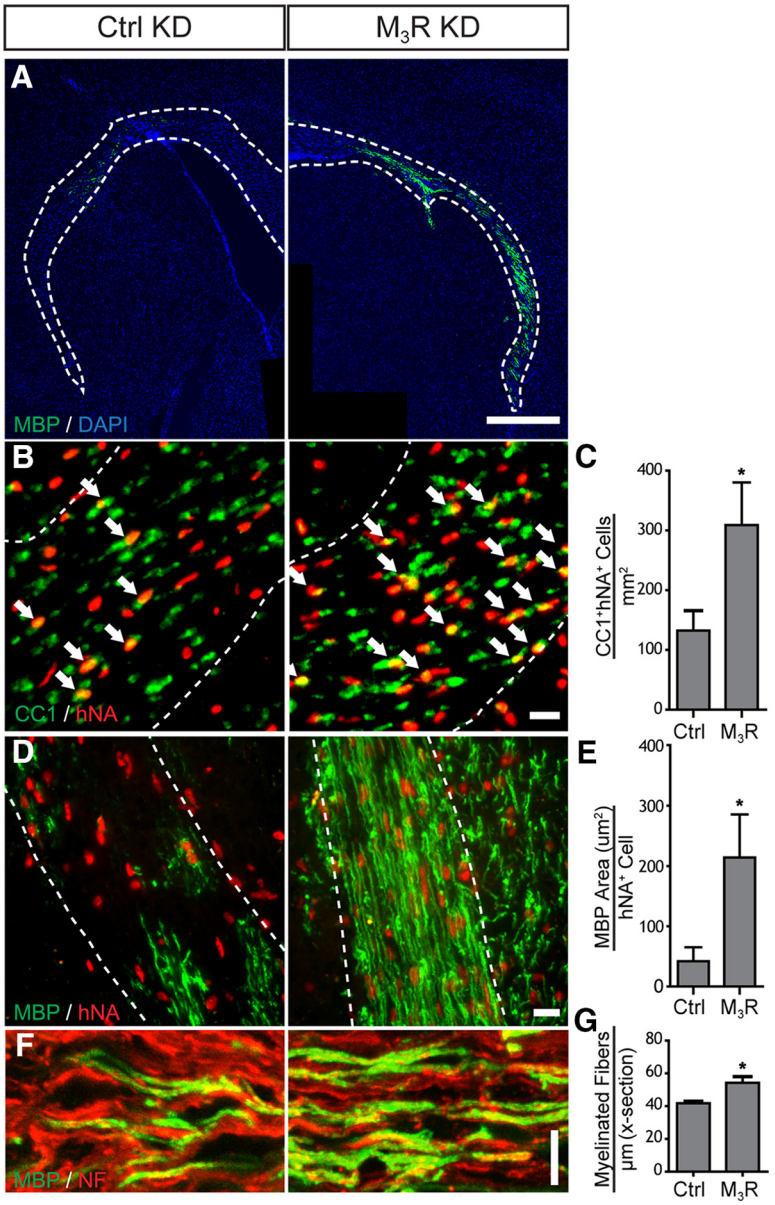


**Figure 3.** Long-term LV KD of $M_3R$ promotes remyelination by transplanted hOPCs. *Shiverer/rag2* pups were transplanted with hOPCs following LV infection and selection. At 12 weeks after implantation, human cells were stained for hNA (red) and MBP (green) (***A***). Immunostaining for differentiated oligodendrocytes (CC1, green) showed that $M_3R$ KD increased the resultant density of human $hNA^+CC1^+$ oligodendrocytes (arrows) in the corpus callosum following engraftment (***B***, quantified in ***C***). Analysis of MBP synthesis revealed that, compared with controls, $M_3R$ KD cells produced substantially more MBP-stained fibers per transplanted cell in the corpus callosum (***D***, quantified in ***E***). Within myelinated regions, $M_3R$ KD led to an increased number of MBP (green) ensheathed axons (neurofilament, red) compared with controls (***F***, quantified in ***G***). Dotted lines indicate outline of the corpus callosum. $^*p < 0.05$ (*t* test). $n = 3$ animals per group, mean ± SEM shown. Scale bars: ***A***, 500 μm; ***B***, 20 μm; ***D***, 10 μm; ***F***, 20 μm.

### $M_{1/3}R$-selective antagonist accelerates oligodendrocyte differentiation during remyelination

While the *shiverer* model is ideal for assessing effects on human oligodendrocyte differentiation and transplant-mediated myelination, the *shiverer* hypomyelinating environment is not a model of demyelination. We therefore tested whether $M_3R$ regulates oligodendrocyte differentiation following lysolecithin-induced demyelination in mouse spinal cord. We initially tested whether a selective $M_1/M_3R$ antagonist (solifenacin) would enhance oligodendrocyte differentiation in a similar manner to clemastine (Mei et al., 2014), which can potently antagonize several GPCRs (Nörenberg et al., 2011; Gregori-Puigjané et al., 2012). Demyelination was induced in adult mouse spinal cord by injection of lysolecithin into the dorsal funiculus and ventrolateral white matter. Animals received solifenacin (10 mg/kg daily, s.c.) or saline daily until death at 14 dpl, during the onset of remyelination in this model (Fancy et al., 2009, 2011). Solifenacin treatment increased the density of *Plp1*-positive oligodendrocytes at 14 dpl compared with saline-treated controls (Fig. 4; solifenacin: 1211 ± 68 vs saline: 836 ± 45 cells/$mm^2$, *t* test $p = 0.02$, $n = 3$). Similarly, solifenacin treatment increased the density of $CC1^+$ oligodendrocytes by immunofluorescence (Fig. 4*B*,*G*; solifenacin: 1224 ± 46 vs saline: 1016 ± 56 cells/$mm^2$, *t* test $p = 0.04$, $n = 3$). Interestingly, we found no difference in $Olig2^+$ oligodendrocyte lineage cell density (Fig. 4*C*,*H*; saline: 1643 ± 207.9 cells/$mm^2$; solifenacin: 1627 ± 267.9 cells/$mm^2$, $p = 0.97$, $n = 3$), suggesting that solifenacin similarly enhanced differentiation. Solifenacin treatment did not influence lesion size (data not shown), microglial response (Iba1, Fig. 4*D*), or astrogliosis

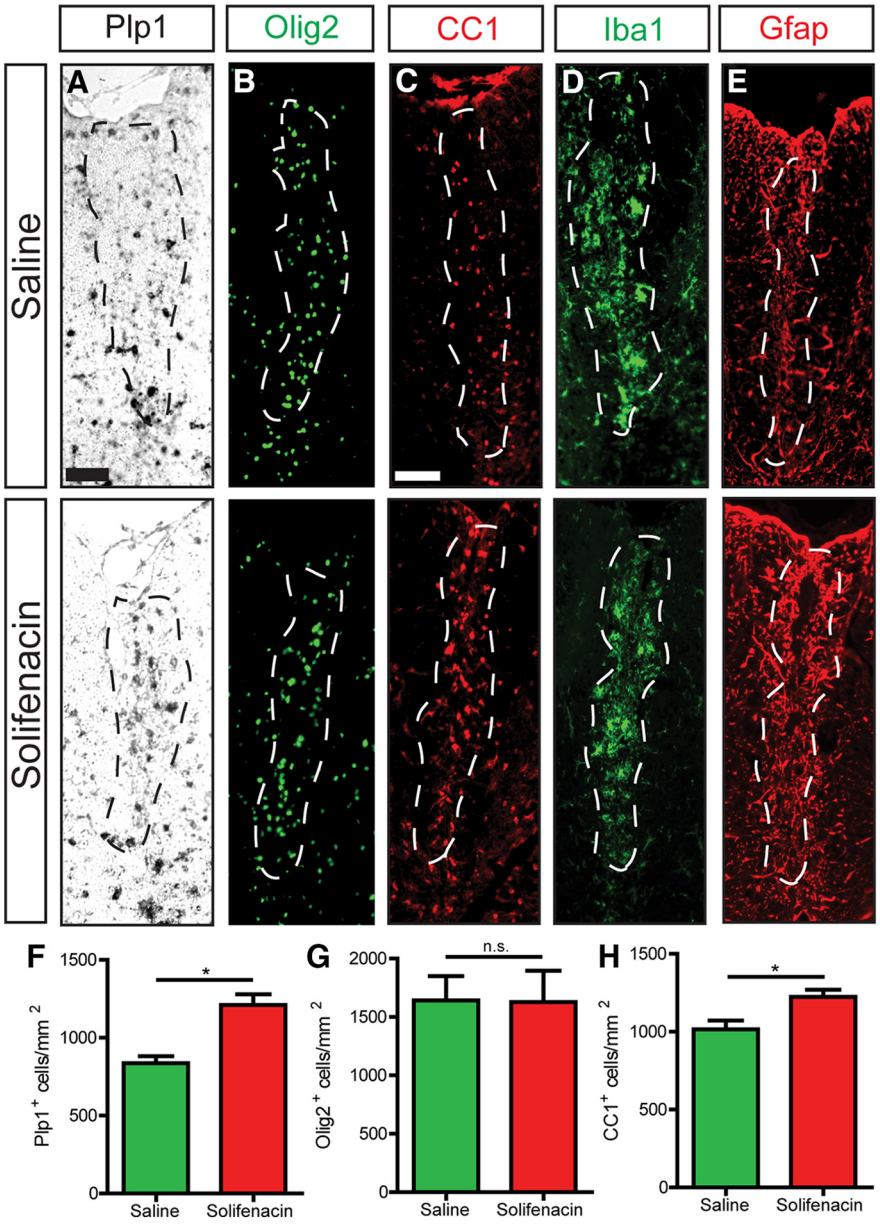


**Figure 4.** Systemic solifenacin treatment enhances OPC differentiation following focal demyelination of mouse spinal cord. Young adult (8- to 10-week-old) mouse spinal cords were lesioned via direct injection of lysolecithin into dorsal white matter. Animals received daily subcutaneous administration of either isotonic saline (top row) or 10 mg/kg solifenacin (bottom row) from day of lesion until death at 14 dpl. *In situ* hybridization for *Plp1* (***A***, quantified in ***F***) and CC1 immunostaining (***C***, quantified in ***H***) revealed increased density of oligodendrocytes in solifenacin animals relative to controls (quantified in ***F*** and ***H***, respectively) with no observable effect on overall density of oligodendrocyte lineage cells (Olig2 in ***B***, quantified in ***G***), microglial response (Iba1, ***D***), or astrogliosis (Gfap, ***E***). $^*p < 0.05$ (Student's *t* test). $n = 3$ per group, mean ± SEM shown. Scale bars: ***A***, ***B***, 40 μm; ***C–E***, 100 μm.

(GFAP, Fig. 4*E*) compared with saline ($n = 3$). These results suggest that $M_{1/3}$R selective antagonists have therapeutic potential and are consistent with a role for either $M_1$R or $M_3$R in OPC and oligodendrocyte differentiation.

### Conditional knock-out of $M_3$R in adult OPCs accelerates oligodendrocyte differentiation and remyelination following demyelination

Based on the role of $M_3$R in human progenitors and solifenacin treatment during remyelination, we hypothesized that conditional $M_3$R knock-out in adult OPCs would be sufficient to increase oligodendrocyte differentiation and remyelination and that this would not be compensated by $M_1$R signaling. To test this hypothesis, we investigated the effect of conditional $M_3$R deletion from adult NG2-expressing OPCs (Fig. 5). We generated homozygous *NG2CreER$^{T2}$:M$_3$R$^{fl/fl}$:Rosa26-Yfp* ($M_3$R-inducible conditional knock-out [icKO]) mice to ask whether $M_3$R deletion in NG2$^+$PDGFαR$^+$ OPCs could accelerate oligodendrocyte differentiation in a solifenacin-like manner. Tamoxifen was administered for 5 d to 8- to 9-week-old mice, and lysolecithin demyelinating lesions were induced 7 d after the last injection to ensure clearance of tamoxifen ($n = 4$ animals per group). To assess the role of $M_3$R signaling on OPC differentiation, mice were killed at 14 dpl. Consistent with previous reports (Zhu et al., 2011), we observed YFP expression in 54.6 ± 6.1% of Olig2$^+$ oligodendrocyte lineage cells, suggesting a relatively high rate of cre-mediated recombination ($n = 4$).

Next, we assessed the overall effect of *M$_3$R* icKO in NG2-expressing OPCs on oligodendrocyte differentiation. *M$_3$R* icKO substantially increased the density of *Plp1*$^+$ oligodendrocytes in 14 dpl lesions relative to controls (Fig. 5*A*,*B*; wild-type [WT]: 599.8 ± 59.9 cells/mm$^2$, $n = 5$; icKO: 791 ± 49 cells/mm$^2$, $n = 4$, $p = 0.04$). This was not accompanied by a reduction in Olig2$^+$ cell density, suggesting that the effect of $M_3$R ablation was due to induced differentiation (Fig. 5*C*,*D*; WT: 1072 ± 155 cells/mm$^2$; icKO: 1117 ± 56 cells/mm$^2$, $n = 4$, $p = 0.8$). Consistent with this interpretation, we observed that a significantly greater proportion of Olig2$^+$ cells were CC1$^+$ oligodendrocytes in icKO animals relative to controls (Fig. 5*E*,*F*; WT: 54.9 ± 5.7% CC1$^+$/Olig2$^+$; icKO 70.4 ± 2.0% CC1$^+$/Olig2$^+$, $p = 0.04$, $n = 4$). Importantly, we found that the majority of CC1$^+$ oligodendrocytes also expressed YFP$^+$ (54.9 ± 0.5%, $n = 3$), indicating that they had undergone cre-mediated recombination. In addition, we observed a cell-autonomous mechanism of $M_3$R on OPC differentiation. A greater proportion of recombined (YFP$^+$) oligodendrocyte lineage cells differentiated to CC1$^+$ oligodendrocytes compared with nonrecombined OPCs (CC1$^+$YFP$^+$/YFP$^+$: 73.7 ± 3.3% CC1$^+$; CC1$^+$YFP$^-$/YFP$^-$: 57.1 ± 3.2% CC1$^+$, $p = 0.02$, $n = 3$). We found no difference in Iba1 immunolabeling of microglia (Fig. 5*G*) or in GFAP immunostaining for astrocytes (Fig. 5*H*) between icKO and WT groups. To assess the effect of *M$_3$R* icKO on OPC recruitment to demyelinated lesions, we euthanized mice at 5 dpl and determined oligodendrocyte lineage density by Olig2 immunostaining. We found no significant difference in Olig2$^+$ cell density between WT and icKO animals (WT: 522 ± 84 cells/mm$^2$; icKO: 604 ± 59 cells/mm$^2$, $n = 3$, $p = 0.47$). These data indicate that ablation of $M_3$R signaling in OPCs enhances their differentiation with no effect on recruitment, po-

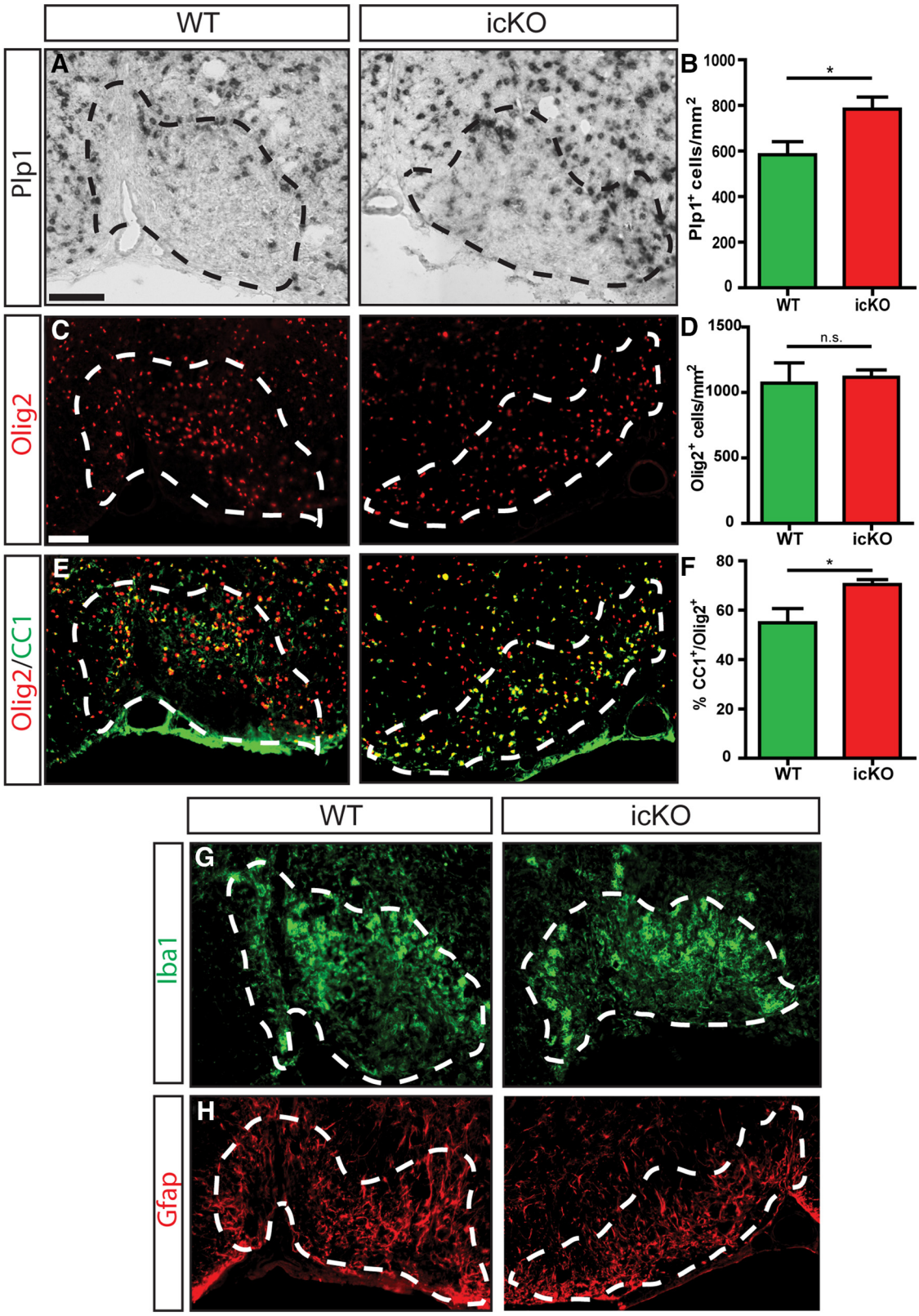


**Figure 5.** Conditional $M_3$R knock-out in OPCs enhances their differentiation following focal demyelination of mouse spinal cords. Genetic ablation of $M_3$R in NG2$^+$ OPCs was induced in *NG2CreER$^{T2}$:Rosa-YFP:M$_3$R$^{fl/fl}$* young adult (8- to 10-week-old) mice via daily intraperitoneal injection of 200 mg/kg tamoxifen. Mice received either tamoxifen or canola oil (vehicle) for 5 d, and their spinal cords were lesioned via direct injection of lysolecithin 1 week after the final day of intraperitoneal injections. Animals were killed at 14 dpl, and spinal cord tissue was collected for histological analysis. *In situ* hybridization for *Plp1* revealed increased oligodendrocyte density in *M$_3$R* icKO animals relative to WT controls (***A***, quantified in ***B***). We observed a significantly greater proportion of oligodendrocyte lineage cells that were oligodendrocytes in *M$_3$R* icKO animals relative to controls (immunostaining for CC1 in ***E***, quantified in ***F***). *M$_3$R* deletion did not influence the overall density of oligodendrocyte lineage cells (Olig2 in ***C***, quantified in ***D***). OPC-specific conditional *M$_3$R* knock-out had no observable effect on microglial response (Iba1, ***G***) or astrogliosis (Gfap, ***H***). *$p < 0.05$ (Student's *t* test). $n = 4$ or 5 per group, mean ± SEM shown. Scale bar, 200 $\mu$m.

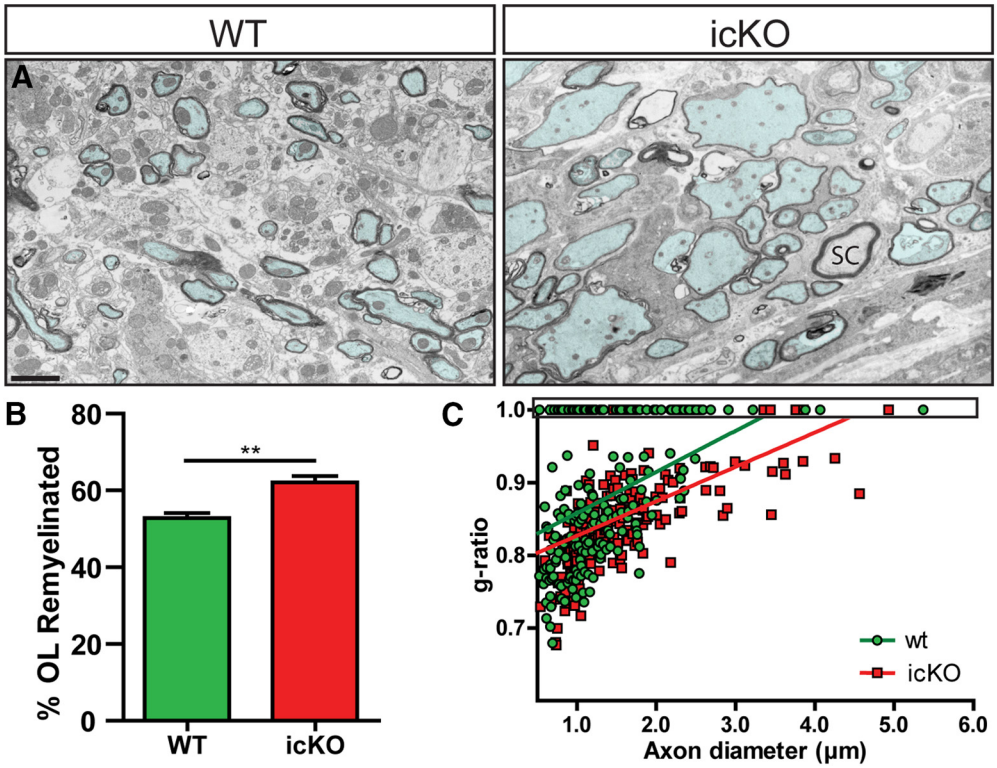


**Figure 6.** Conditional ablation of $M_3R$ in OPCs accelerates remyelination. OPC-specific $M_3R$ knock-out was induced in adult *NG2CreER$^{T2}$:Rosa-YFP:M$_3$R$^{fl/fl}$* mice by daily intraperitoneal administration of 200 mg/kg tamoxifen or vehicle for 5 d. Animals were lesioned 1 week after the last day of injection. Animals were killed at 14 dpl and spinal cord tissue processed into resin for electron microscopy. Analysis revealed that *$M_3R$* icKO in OPCs significantly increased the proportion of oligodendrocyte (OL) remyelinated axons in lesions compared with WT animals (***A***, quantified in ***B***, mean ± SEM). ***C***, Quantification of myelin sheath thickness in WT (green) and *$M_3R$* iCKO (red) at 14 dpl by g-ratio analysis. SC, Schwann cell-remyelinated fiber. $^{**}p < 0.01$ (Student's *t* test). $n =$ 3 or 4 animals, ≥300 axons per animal. Scale bar, 2 μm.

tentially by inducing more rapid cell cycle exit and terminal differentiation at the cost of proliferation.

To examine whether enhanced differentiation of $M_3R$-deficient OPCs correlated with accelerated remyelination, we repeated our transgenic animal lesion paradigm and processed spinal cords for myelin ultrastructure analysis by electron microscopy. At 14 dpl, during the onset of remyelination, we found that *$M_3R$* icKO significantly increased the proportion of remyelinated axons relative to WT controls (Fig. 6) (WT: 52.9 ± 1.2% remyelinated, $n = 3$; icKO: 62.1 ± 1.7% remyelinated, $n = 4$, $p =$ 0.009). Consistent with an acceleration of OPC differentiation, and remyelination following *$M_3R$* icKO, myelin *g*-ratio analysis revealed significantly decreased *g*-ratio, which represents the relative thickness of myelin in remyelinated fibers compared with axonal diameter (Fig. 6*C*). Together, these data demonstrate that $M_3R$ signaling in OPCs delays efficient remyelination in adult spinal cord.

## Discussion

In this paper, we demonstrate that $M_3R$ signaling acts to delay OPC differentiation and ultimately contributes to delayed remyelination. We found that $M_3R$ signaling is functionally important and conserved in both mouse and human progenitors. The net effect of inhibition of muscarinic signaling is the acceleration of OPC and oligodendrocyte differentiation, leading to improved remyelination and myelin repair. In hOPCs transduced with KD virus or murine OPCs with conditional knock-out, $M_3R$ ablation alone was sufficient to induce precocious oligodendrocyte differentiation. Furthermore, fate-mapping of *$M_3R$*-null OPCs confirmed that this was mediated by a cell-autonomous mechanism.

While the functional importance of specific MR subtypes in OPCs is not known, recent data indicate that $M_1R$ plays a key role in the maturation of immature oligodendrocytes (Mei et al., 2016). While we did not assess the role of $M_1R$ directly in this study, Mei et al. (2016) reported negative results using oligodendrocyte lineage cells isolated from germline *$M_3R$* knock-out mice. The apparent difference between these studies might be due to compensatory changes that occur following germline deletion in neural stem cells versus specific ablation in OPCs or due to differences in the developmental stages of cells examined *in vitro*. Mei et al. (2016) isolated mouse progenitors/immature oligodendrocytes using O4 from postnatal day 7 mouse brain, which represents a later stage of oligodendrocyte development than the human fetal CD140a/PDGFαR$^+$ used in the current study. Likewise, conditional deletion of $M_1R$ was achieved using the CNP-cre mouse (Lappe-Siefke et al., 2003), which drives recombination primarily in immature oligodendrocytes after the formation of OPCs (Ye et al., 2009). Thus, it appears that the role of $M_3R$ is restricted to earlier PDGFαR/NG2 stages of the oligodendrocyte lineage, whereas $M_1R$ regulates differentiation in committed progenitors and immature oligodendrocytes. Direct comparison of conditional KO mice using the same cre driver lines and the use of CRISPR-mediated deletion of $M_1R$ and $M_3R$ in human IPSCs will provide a more definitive understanding of the contribution of these inhibitory receptors.

The pattern of MR subtype mRNA expression is different between human and mouse OPCs, and the reported effects of MR agonists on proliferation appear to be different between species (Cohen et al., 1996; De Angelis et al., 2012; Abiraman et al., 2015). Our data indicate that $M_3R$ is critical for calcium-related signal-

ing induced by muscarinic agonists in OPCs, suggesting that, at least in human primary OPCs, $M_3R$ is the operant receptor. Quantitative differences in expression signature and specifically in receptor subtype expression likely underlie some of the differences observed between human and rodent (Sim et al., 2009; Dietz et al., 2016). Such differences will be of upmost importance when designing therapeutic approaches that target signaling pathways to be translated from preclinical to human patients.

Interestingly, MR expression is highly variable within the FACS-isolated $CD140a^+/O4^+$ hOPC population with at least one-fourth of hOPCs expressing high levels of $M_3R$/CHRM3 mRNA. Along with similar heterogeneity of other neurotransmitter receptor expression, it appears that a mosaic of OPCs in fetal forebrain exist with differing responsiveness to environmental and neuronal stimuli. Whether the variability in $M_3R$ expression represents stochastic expression within a single population of hOPCs or is representative of a specific stage of oligodendrocyte lineage differentiation remains to be determined. Intriguingly, a direct comparison of $M_3R$-positive and $M_3R$-negative hOPCs identified $G\alpha_q$-associated transcripts as the most significantly regulated gene set among pathways in the mSigDB ($q = 1.33 \times 10^{-7}$; ST_GAQ_PATHWAY) (Subramanian et al., 2005). This may suggest that $M_3R$-expressing hOPCs are primed to respond via M3R/$G\alpha_q$-coupled signaling.

The muscarinic antagonist clemastine is under active clinical investigation as a remyelinating agent in MS (www.clinicaltrials.gov, NCT02040298 and NCT02521311). Clemastine has shown great promise in mouse models of demyelination and MS (Mei et al., 2014, 2016; Liu et al., 2016). However, there are some concerns that centrally acting nonspecific MR antagonists induce cognitive impairment due to inhibition of $M_1R$ signaling (Anagnostaras et al., 2003). Furthermore, the use of antimuscarinic agents is associated with mild cognitive impairment and dementia in the aging population (Cai et al., 2013). $M_1R$ is the most abundant subtype in forebrain and hippocampus (Levey et al., 1995). $M_1R$ expression is decreased in schizophrenia (Dean et al., 2002), and MR antagonists have been shown to worsen Alzheimer's disease (Perry et al., 2003). Together, these findings suggest that $M_1R$-acting drugs may not be optimal targets for MS therapy. On the other hand, $M_3R$ antagonists are typically well tolerated clinically with a manageable peripheral side effect profile (Chapple, 2006). It is not clear whether $M_3R$-selective antagonists would avoid the cognitive adverse side effects. As such, the development of new selective and potent $M_3R$ antagonists might yield an effective approach to improve both spontaneous and transplant-mediated repair while minimizing CNS anticholinergic side effects.

The cellular source of ACh that activates $M_{1/3}R$ following demyelination and impairs OPC differentiation and remyelination is unknown. ACh fibers are widely distributed in the forebrain and spinal cord, and both axons and dendrites have the capability to release ACh (Garzón and Pickel, 2000). Moreover, these fibers can signal extrasynaptically via volume-based neurotransmission (Yamasaki et al., 2010). The differential pattern of acetylcholinesterase and ChAT activity in human brain development (Court et al., 1993) suggests that neuron-derived ACh may act directly on OPC-expressed MRs. OPC differentiation is modulated by $M_{1/3}R$ antagonists in corpus callosum (Deshmukh et al., 2013; Abiraman et al., 2015), midbrain (Abiraman et al., 2015), and spinal cord (Deshmukh et al., 2013; Mei et al., 2014). This is consistent with a widespread role for ACh/MR signaling in OPCs throughout the CNS. However, we cannot rule out other cellular sources of Ach, such as lymphocytes (Kawashima et al., 1989; Rinner and Schauenstein, 1993).

Muscarinic agonist treatment increases $InsP_3$ and $[Ca^{2+}]_i$ in OPCs (Cohen and Almazan, 1994). In this study, we developed a new viral GCaMP6s reporter under the control of EF1$\alpha$ to visualize $Ca^{2+}$ signaling in individual hOPCs. CD140a-sorted hOPCs did not exhibit spontaneous calcium waves *in vitro*. Although we did not attempt to measure rare and small-magnitude calcium events that can occur in OPCs (Haak et al., 2001), we did not observe spontaneous $Ca^{2+}$ waves that have been described in migrating murine OPCs grown in serum-containing media (Paez et al., 2009). The lack of spontaneous $Ca^{2+}$ waves allowed us to determine whether increased $[Ca^{2+}]_i$ is regulated by $M_1R$ and/or $M_3R$, both $G_q$-coupled receptors. $M_3R$ KD largely inhibited muscarinic agonist increased $[Ca^{2+}]_i$, suggesting that $M_3R$ is the principal mediator of this response in $CD140a^+$ hOPCs. The possibility that MR-coupled $Ca^{2+}$ signaling directly contributes to the inhibition of OPC differentiation represents an intriguing contrast to the role of $Ca^{2+}$ entry via voltage-operated calcium channels (Cheli et al., 2015) or calcium-permeable glutamate channels (Wake et al., 2011; Lundgaard et al., 2013) that are known to induce differentiation. Thus, neuronal activity, which drives OPC proliferation and differentiation in the developing brain (Barres and Raff, 1993; Gibson et al., 2014), may act in a neurotransmitter-specific manner to regulate diverse $Ca^{2+}$-dependent signals to it turn regulate OPC homeostasis. The spatiotemporal regulation of $Ca^{2+}$ entry provides the basis for activation of distinct signaling stimuli (Di Capite et al., 2009), with store-operated calcium entry being coupled with $G_q$-coupled GPCRs, such as $M_3R$. It therefore noteworthy that store-operated calcium entry via TRPC1 blocks OPC differentiation (Paez et al., 2011).

The mechanisms that match OPC number to white matter volume are not well understood. In primate development, before OPC specification, the subventricular zone splits into two distinct regions separated by cholinergic fibers emanating from the ganglionic eminence (Smart et al., 2002). Moreover, a distinct population of cholinergic interneurons has been identified in the rodent SVZ (Paez-Gonzalez et al., 2014). As such, cholinergic signaling is well placed to prevent premature OPC differentiation and allow for sufficient proliferation of the progenitors needed for a larger volume of white matter. Cholinergic signals may act to prevent premature demyelination, which would limit the number of progenitors and delay colonization of larger tissue/lesion volume necessary for human development and remyelination in disease.

Finally, by genetically deleting $M_3Rs$ in human cells, we could engineer cells before transplantation to eliminate this otherwise inhibitory environmental cue. Lentiviral-mediated mCherry expression in hOPCs continues for at least 1 year after transplantation, suggesting that *ex vivo* manipulation can modify hOPC gene expression for extended periods of time. While we did not directly assess $M_3R$ KD after transplantation, leaving open the possibility that shRNAi expression may decline, KD of inhibitory $M_3R$ signaling substantially augmented human oligodendrocyte formation over an 8 week period. This type of *ex vivo* genetic modification may represent an important means by which transplanted cells could overcome the inhibitory environment present in most MS lesions. As such, we have established a proof-of-principle that rendering OPCs unresponsive to potentially negative environmental stimuli before implantation represents a viable approach to increase the capacity for remyelination by transplanted hOPCs. $M_1R$ and $M_3R$ are representative of an

emerging set of pharmacological targets that relay inhibitory signals for differentiation in demyelination and may be targeted to improve remyelination MS lesions.

## References


Abiraman K, Pol SU, O'Bara MA, Chen GD, Khaku ZM, Wang J, Thorn D, Vedia BH, Ekwegbalu EC, Li JX, Salvi RJ, Sim FJ (2015) Anti-muscarinic adjunct therapy accelerates functional human oligodendrocyte repair. J Neurosci 35:3676–3688. CrossRef Medline

Anagnostaras SG, Murphy GG, Hamilton SE, Mitchell SL, Rahnama NP, Nathanson NM, Silva AJ (2003) Selective cognitive dysfunction in acetylcholine M1 muscarinic receptor mutant mice. Nat Neurosci 6:51–58. CrossRef Medline

Barres BA, Raff MC (1993) Proliferation of oligodendrocyte precursor cells depends on electrical activity in axons. Nature 361:258–260. CrossRef Medline

Cai X, Campbell N, Khan B, Callahan C, Boustani M (2013) Long-term anticholinergic use and the aging brain. Alzheimers Dement 9:377–385. CrossRef Medline

Chapple CR (2006) Solifenacin provides effective antimuscarinic therapy for the complete management of overactive bladder. Expert Opinion Pharmacother 7:2421–2434. CrossRef Medline

Cheli VT, Santiago González DA, Spreuer V, Paez PM (2015) Voltage-gated $Ca^{2+}$ entry promotes oligodendrocyte progenitor cell maturation and myelination in vitro. Exp Neurol 265:69–83. CrossRef Medline

Chen TW, Wardill TJ, Sun Y, Pulver SR, Renninger SL, Baohan A, Schreiter ER, Kerr RA, Orger MB, Jayaraman V, Looger LL, Svoboda K, Kim DS (2013) Ultrasensitive fluorescent proteins for imaging neuronal activity. Nature 499:295–300. CrossRef Medline

Cohen RI, Almazan G (1994) Rat oligodendrocytes express muscarinic receptors coupled to phosphoinositide hydrolysis and adenylyl cyclase. Eur J Neurosci 6:1213–1224. CrossRef Medline

Cohen RI, Molina-Holgado E, Almazan G (1996) Carbachol stimulates c-fos expression and proliferation in oligodendrocyte progenitors. Brain Res Mol Brain Res 43:193–201. CrossRef Medline

Conway GD, O'Bara MA, Vedia BH, Pol SU, Sim FJ (2012) Histone deacetylase activity is required for human oligodendrocyte progenitor differentiation. Glia 60:1944–1953. CrossRef Medline

Court JA, Perry EK, Johnson M, Piggott MA, Kerwin JA, Perry RH, Ince PG (1993) Regional patterns of cholinergic and glutamate activity in the developing and aging human brain. Brain Res Dev Brain Res 74:73–82. CrossRef Medline

Dean B, McLeod M, Keriakous D, McKenzie J, Scarr E (2002) Decreased muscarinic1 receptors in the dorsolateral prefrontal cortex of subjects with schizophrenia. Mol Psychiatry 7:1083–1091. CrossRef Medline

De Angelis F, Bernardo A, Magnaghi V, Minghetti L, Tata AM (2012) Muscarinic receptor subtypes as potential targets to modulate oligodendrocyte progenitor survival, proliferation, and differentiation. Dev Neurobiol 72:713–728. CrossRef Medline

Deshmukh VA, Tardif V, Lyssiotis CA, Green CC, Kerman B, Kim HJ, Padmanabhan K, Swoboda JG, Ahmad I, Kondo T, Gage FH, Theofilopoulos AN, Lawson BR, Schultz PG, Lairson LL (2013) A regenerative approach to the treatment of multiple sclerosis. Nature 502:327–332. CrossRef Medline

Di Capite J, Ng SW, Parekh AB (2009) Decoding of cytoplasmic Ca(2+) oscillations through the spatial signature drives gene expression. Curr Biol 19:853–858. CrossRef Medline

Dietz KC, Polanco JJ, Pol SU, Sim FJ (2016) Targeting human oligodendrocyte progenitors for myelin repair. Exp Neurol 283:489–500. CrossRef Medline

Dörje F, Wess J, Lambrecht G, Tacke R, Mutschler E, Brann MR (1991) Antagonist binding profiles of five cloned human muscarinic receptor subtypes. J Pharmacol Exp Ther 256:727–733. Medline

Edelstein A, Amodaj N, Hoover K, Vale R, Stuurman N (2010) Computer control of microscopes using microManager. Curr Protoc Mol Biol 14: Unit 14.20. CrossRef Medline

Fancy SP, Zhao C, Franklin RJ (2004) Increased expression of Nkx2.2 and Olig2 identifies reactive oligodendrocyte progenitor cells responding to demyelination in the adult CNS. Mol Cell Neurosci 27:247–254. CrossRef Medline

Fancy SP, Baranzini SE, Zhao C, Yuk DI, Irvine KA, Kaing S, Sanai N, Franklin RJ, Rowitch DH (2009) Dysregulation of the wnt pathway inhibits timely myelination and remyelination in the mammalian CNS. Genes Dev 23:1571–1585. CrossRef Medline

Fancy SP, Harrington EP, Yuen TJ, Silbereis JC, Zhao C, Baranzini SE, Bruce CC, Otero JJ, Huang EJ, Nusse R, Franklin RJ, Rowitch DH (2011) Axin2 as regulatory and therapeutic target in newborn brain injury and remyelination. Nat Neurosci 14:1009–1016. CrossRef Medline

Franklin RJ, Goldman SA (2015) Glia disease and repair-remyelination. Cold Spring Harb Perspect Biol 7:a020594. CrossRef Medline

Garzón M, Pickel VM (2000) Dendritic and axonal targeting of the vesicular acetylcholine transporter to membranous cytoplasmic organelles in laterodorsal and pedunculopontine tegmental nuclei. J Comp Neurol 419: 32–48. CrossRef Medline

Gautam D, Han SJ, Hamdan FF, Jeon J, Li B, Li JH, Cui Y, Mears D, Lu H, Deng C, Heard T, Wess J (2006) A critical role for beta cell M3 muscarinic acetylcholine receptors in regulating insulin release and blood glucose homeostasis in vivo. Cell Metab 3:449–461. CrossRef Medline

Geraerts M, Willems S, Baekelandt V, Debyser Z, Gijsbers R (2006) Comparison of lentiviral vector titration methods. BMC Biotechnol 6:34. CrossRef Medline

Gibson EM, Purger D, Mount CW, Goldstein AK, Lin GL, Wood LS, Inema I, Miller SE, Bieri G, Zuchero JB, Barres BA, Woo PJ, Vogel H, Monje M (2014) Neuronal activity promotes oligodendrogenesis and adaptive myelination in the mammalian brain. Science 344:1252304. CrossRef Medline

Gregori-Puigjané E, Setola V, Hert J, Crews BA, Irwin JJ, Lounkine E, Marnett L, Roth BL, Shoichet BK (2012) Identifying mechanism-of-action targets for drugs and probes. Proc Natl Acad Sci U S A 109:11178–11183. CrossRef Medline

Haak LL, Song LS, Molinski TF, Pessah IN, Cheng H, Russell JT (2001) Sparks and puffs in oligodendrocyte progenitors: cross talk between ryanodine receptors and inositol trisphosphate receptors. J Neurosci 21: 3860–3870. CrossRef Medline

Huang JK, Fancy SP, Zhao C, Rowitch DH, Ffrench-Constant C, Franklin RJ (2011a) Myelin regeneration in multiple sclerosis: targeting endogenous stem cells. Neurotherapeutics 8:650–658. CrossRef Medline

Huang JK, Jarjour AA, Nait Oumesmar B, Kerninon C, Williams A, Krezel W, Kagechika H, Bauer J, Zhao C, Baron-Van Evercooren A, Chambon P, Ffrench-Constant C, Franklin RJ (2011b) Retinoid X receptor gamma signaling accelerates CNS remyelination. Nat Neurosci 14:45–53. CrossRef Medline

Irvine KA, Blakemore WF (2008) Remyelination protects axons from demyelination-associated axon degeneration. Brain 131:1464–1477. CrossRef Medline

Kawashima K, Oohata H, Fujimoto K, Suzuki T (1989) Extraneuronal localization of acetylcholine and its release upon nicotinic stimulation in rabbits. Neurosci Lett 104:336–339. CrossRef Medline

Kuhlmann T, Miron V, Cui Q, Wegner C, Antel J, Brück W (2008) Differentiation block of oligodendroglial progenitor cells as a cause for remyelination failure in chronic multiple sclerosis. Brain 131:1749–1758. CrossRef Medline

Lappe-Siefke C, Goebbels S, Gravel M, Nicksch E, Lee J, Braun PE, Griffiths IR, Nave KA (2003) Disruption of Cnp1 uncouples oligodendroglial functions in axonal support and myelination. Nat Genet 33:366–374. CrossRef Medline

Levey AI, Edmunds SM, Koliatsos V, Wiley RG, Heilman CJ (1995) Expression of m1–m4 muscarinic acetylcholine receptor proteins in rat hippocampus and regulation by cholinergic innervation. J Neurosci 15: 4077–4092. CrossRef Medline

Liu J, Dupree JL, Gacias M, Frawley R, Sikder T, Naik P, Casaccia P (2016) Clemastine enhances myelination in the prefrontal cortex and rescues behavioral changes in socially isolated mice. J Neurosci 36:957–962. CrossRef Medline

Lundgaard I, Luzhynskaya A, Stockley JH, Wang Z, Evans KA, Swire M, Volbracht K, Gautier HO, Franklin RJ, Charles FC, Attwell D, Káradóttir RT (2013) Neuregulin and BDNF induce a switch to NMDA receptor-dependent myelination by oligodendrocytes. PLoS Biol 11:e1001743. CrossRef Medline

Mei F, Fancy SP, Shen YA, Niu J, Zhao C, Presley B, Miao E, Lee S, Mayoral SR, Redmond SA, Etxeberria A, Xiao L, Franklin RJ, Green A, Hauser SL, Chan JR (2014) Micropillar arrays as a high-throughput screening platform for therapeutics in multiple sclerosis. Nat Med 20:954–960. CrossRef Medline

Mei F, Lehmann-Horn K, Shen YA, Rankin KA, Stebbins KJ, Lorrain DS, Pekarek K, A Sagan S,Xiao L, Teuscher C, von Büdingen HC, Wess J, Lawrence JJ, Green AJ, Fancy SP, Zamvil SS, Chan JR (2016) Accelerated remyelination during inflammatory demyelination prevents axonal loss and improves functional recovery. Elife 5:e18246. CrossRef Medline

Najm FJ, Madhavan M, Zaremba A, Shick E, Karl RT, Factor DC, Miller TE, Nevin ZS, Kantor C, Sargent A, Quick KL, Schlatzer DM, Tang H, Papoian R, Brimacombe KR, Shen M, Boxer MB, Jadhav A, Robinson AP, Podojil JR, et al. (2015) Drug-based modulation of endogenous stem cells promotes functional remyelination in vivo. Nature 522:216–220. CrossRef Medline

Nörenberg W, Hempel C, Urban N, Sobottka H, Illes P, Schaefer M (2011) Clemastine potentiates the human P2X7 receptor by sensitizing it to lower ATP concentrations. J Biol Chem 286:11067–11081. CrossRef Medline

Paez PM, Fulton DJ, Spreuer V, Handley V, Campagnoni CW, Macklin WB, Colwell C, Campagnoni AT (2009) Golli myelin basic proteins regulate oligodendroglial progenitor cell migration through voltage-gated $Ca^{2+}$ influx. J Neurosci 29:6663–6676. CrossRef Medline

Paez PM, Fulton D, Spreuer V, Handley V, Campagnoni AT (2011) Modulation of canonical transient receptor potential channel 1 in the proliferation of oligodendrocyte precursor cells by the golli products of the myelin basic protein gene. J Neurosci 31:3625–3637. CrossRef Medline

Paez-Gonzalez P, Asrican B, Rodriguez E, Kuo CT (2014) Identification of distinct ChAT(+) neurons and activity-dependent control of postnatal SVZ neurogenesis. Nature Neuroscience 17:934–942. CrossRef Medline

Perry EK, Kilford L, Lees AJ, Burn DJ, Perry RH (2003) Increased Alzheimer pathology in Parkinson's disease related to antimuscarinic drugs. Ann Neurol 54:235–238. CrossRef Medline

Pol SU, Lang JK, O'Bara MA, Cimato TR, McCallion AS, Sim FJ (2013) Sox10-MCS5 enhancer dynamically tracks human oligodendrocyte progenitor fate. Exp Neurol 247:694–702. CrossRef Medline

Ragheb F, Molina-Holgado E, Cui QL, Khorchid A, Liu HN, Larocca JN, Almazan G (2001) Pharmacological and functional characterization of muscarinic receptor subtypes in developing oligodendrocytes. J Neurochem 77:1396–1406. CrossRef Medline

Rinner I, Schauenstein K (1993) Detection of choline-acetyltransferase activity in lymphocytes. J Neurosci Res 35:188–191. CrossRef Medline

Schindelin J, Arganda-Carreras I, Frise E, Kaynig V, Longair M, Pietzsch T, Preibisch S, Rueden C, Saalfeld S, Schmid B, Tinevez JY, White DJ, Hartenstein V, Eliceiri K, Tomancak P, Cardona A (2012) Fiji: an open-source platform for biological-image analysis. Nat Methods 9:676–682. CrossRef Medline

Sevin C, Benraiss A, Van Dam D, Bonnin D, Nagels G, Verot L, Laurendeau I, Vidaud M, Gieselmann V, Vanier M, De Deyn PP, Aubourg P, Cartier N (2006) Intracerebral adeno-associated virus-mediated gene transfer in rapidly progressive forms of metachromatic leukodystrophy. Hum Mol Genet 15:53–64. CrossRef Medline

Sim FJ, Zhao C, Penderis J, Franklin RJ (2002) The age-related decrease in CNS remyelination efficiency is attributable to an impairment of both oligodendrocyte progenitor recruitment and differentiation. J Neurosci 22:2451–2459. CrossRef Medline

Sim FJ, Windrem MS, Goldman SA (2009) Fate determination of adult human glial progenitor cells. Neuron Glia Biol 5:45–55. CrossRef Medline

Sim FJ, McClain CR, Schanz SJ, Protack TL, Windrem MS, Goldman SA (2011) CD140a identifies a population of highly myelinogenic, migration-competent and efficiently engrafting human oligodendrocyte progenitor cells. Nat Biotechnol 29:934–941. CrossRef Medline

Sim F, Lang J, Waldau B, Roy N, Schwartz T, Pilcher W, Chandross K, Natesan S, Merrill J, Goldman S (2006) Complementary patterns of gene expression by human oligodendrocyte progenitors and their environment predict determinants of progenitor maintenance and differentiation. Ann Neurol 59:763–779. CrossRef Medline

Smart IH, Dehay C, Giroud P, Berland M, Kennedy H (2002) Unique morphological features of the proliferative zones and postmitotic compartments of the neural epithelium giving rise to striate and extrastriate cortex in the monkey. Cereb Cortex 12:37–53. CrossRef Medline

Subramanian A, Tamayo P, Mootha VK, Mukherjee S, Ebert BL, Gillette MA, Paulovich A, Pomeroy SL, Golub TR, Lander ES, Mesirov JP (2005) Gene set enrichment analysis: a knowledge-based approach for interpreting genome-wide expression profiles. Proc Natl Acad Sci U S A 102:15545–15550. CrossRef Medline

Trapp BD, Nave KA (2008) Multiple sclerosis: an immune or neurodegenerative disorder? Annu Rev Neurosci 31:247–269. CrossRef Medline

Tsai FC, Seki A, Yang HW, Hayer A, Carrasco S, Malmersjö S, Meyer T (2014) A polarized $Ca^{2+}$, diacylglycerol and STIM1 signalling system regulates directed cell migration. Nat Cell Biol 16:133–144. CrossRef Medline

Wake H, Lee PR, Fields RD (2011) Control of local protein synthesis and initial events in myelination by action potentials. Science 333:1647–1651. CrossRef Medline

Wang J, Pol SU, Haberman AK, Wang C, O'Bara MA, Sim FJ (2014) Transcription factor induction of human oligodendrocyte progenitor fate and differentiation. Proc Natl Acad Sci U S A 111:E2885–E2894. CrossRef Medline

Wang S, Bates J, Li X, Schanz S, Chandler-Militello D, Levine C, Maherali N, Studer L, Hochedlinger K, Windrem M, Goldman SA (2013) Human iPSC-derived oligodendrocyte progenitor cells can myelinate and rescue a mouse model of congenital hypomyelination. Cell Stem Cell 12:252–264. CrossRef Medline

Windrem MS, Schanz SJ, Guo M, Tian GF, Washco V, Stanwood N, Rasband M, Roy NS, Nedergaard M, Havton LA, Wang S, Goldman SA (2008) Neonatal chimerization with human glial progenitor cells can both remyelinate and rescue the otherwise lethally hypomyelinated shiverer mouse. Cell Stem Cell 2:553–565. CrossRef Medline

Wolswijk G (1998) Chronic stage multiple sclerosis lesions contain a relatively quiescent population of oligodendrocyte precursor cells. J Neurosci 18:601–609. CrossRef Medline

Yamasaki M, Matsui M, Watanabe M (2010) Preferential localization of muscarinic M1 receptor on dendritic shaft and spine of cortical pyramidal cells and its anatomical evidence for volume transmission. J Neurosci 30:4408–4418. CrossRef Medline

Ye F, Chen Y, Hoang T, Montgomery RL, Zhao XH, Bu H, Hu T, Taketo MM, van Es JH, Clevers H, Hsieh J, Bassel-Duby R, Olson EN, Lu QR (2009) HDAC1 and HDAC2 regulate oligodendrocyte differentiation by disrupting the beta-catenin-TCF interaction. Nat Neurosci 12:829–838. CrossRef Medline

Zeileis A, Grothendieck G (2005) zoo: S3 infrastructure for regular and irregular time series. J Stat Software 14:1–27. CrossRef

Zhang Y, Chen K, Sloan SA, Bennett ML, Scholze AR, O'Keeffe S, Phatnani HP, Guarnieri P, Caneda C, Ruderisch N, Deng S, Liddelow SA, Zhang C, Daneman R, Maniatis T, Barres BA, Wu JQ (2014) An RNA sequencing transcriptome and splicing database of glia, neurons, and vascular cells of the cerebral cortex. J Neurosci 34:11929–11947. CrossRef Medline

Zhao C, Li WW, Franklin RJ (2006) Differences in the early inflammatory responses to toxin-induced demyelination are associated with the age-related decline in CNS remyelination. Neurobiol Aging 27:1298–1307. CrossRef Medline

Zhu X, Hill RA, Dietrich D, Komitova M, Suzuki R, Nishiyama A (2011) Age-dependent fate and lineage restriction of single NG2 cells. Development 138:745–753. CrossRef Medline